A full-configuration-interaction nuclear orbital approach and application for small doped He clusters

M. P. de Lara-Castells, N. F. Aguirre, G. Delgado-Barrio, P. Villarreal, and A. O. Mitrushchenkov

Citation: AIP Conference Proceedings **1642**, 69 (2015); doi: 10.1063/1.4906632
View online: http://dx.doi.org/10.1063/1.4906632
View Table of Contents: http://scitation.aip.org/content/aip/proceeding/aipcp/1642?ver=pdfcov
Published by the AIP Publishing

A Full-Configuration-Interaction Nuclear Orbital Approach and Application for Small Doped He Clusters

M. P. de Lara–Castells*,†, N. F. Aguirre*, G. Delgado–Barrio*, P. Villarreal* and A. O. Mitrushchenkov**

*Instituto de Física Fundamental (CSIC), Serrano 123, 28006 Madrid, Spain
†E-mail: delara@iff.csic.es
**Université Paris-Est, Laboratoire Modélisation et Simulation Multi Echelle, MSME UMR 8208 CNRS, 5 bd Descartes, 77454 Marne-la-Vallée, France

Abstract. An efficient full-configuration-interaction "nuclear orbital" treatment was developed as a benchmark quantum-chemistry-like method to calculate, ground and excited, fermionic "solvent" wave-functions and applied to ^3He_N clusters with atomic or molecular impurities [J. Chem. Phys. (Communication) **125**, 221101 (2006)]. The main difficulty in handling doped ^3He_N clusters lies in the Fermi-Dirac nuclear statistics, the wide amplitudes of the He-dopant and He-He motions, and the hard-core He-He interaction at short distances. This paper overviews the theoretical approach and its recent applications to energetic, structural and spectroscopic aspects of different dopant-^3He_N clusters. Preliminary results by using the latest version of the FCI-NO computational implementation, to bosonic $Cl_2(X)$-$(^4He)_N$ clusters, are also shown.

Keywords: Full Configuration Interaction, quantum solvents, electronic structure, potential energy surfaces, weakly bounded clusters, He nanodroplets, microscopic superfluidity, Raman spectra
PACS: 31.15.A, 31.15.bw, 31.15.ve, 31.15.vj, 31.50.Bc, 31.50.Df, 33.15.Fm, 33.20.Vq

INTRODUCTION

Helium nanodroplets are applied as a weak perturbing cryogenic matrix for high-resolution spectroscopic studies of trapped molecular systems, extracting remarkable information on the quantum solvent as the manifestation of ^{4}He (^{3}He) superfluid (normal fluid) effects and highlighting the key role of bosonic (fermionic) statistical effects. The paradigmatic infrared spectra of a host carbonyl sulfide (OCS) molecule, which depend on the isotope considered, ^{3}He or ^{4}He, represents one of the experimentally most well-documented evidences of the unique properties of He nanodroplets [1, 2]. When OCS is solvated in a bosonic ^{4}He-nanodroplet, the spectrum at 0.37 K is very similar to that of the gas-phase OCS, as the molecule freely rotates. On the contrary, in ^{3}He-nanodroplets, and even at a lower temperature of 0.15 K, the spectrum shows an unstructured broad shape as it occurs in normal liquids. After the addition of a few tenths of ^{4}He atoms, the structured spectrum is recovered, which was considered as the first experimental evidence for the appearance of microscopic superfluidity. Further spectroscopic probes of molecules in rather small doped helium clusters provided insights into the number of ^{4}He atoms which are necessary for the onset of microscopic superfluidity [3, 4, 5, 6, 7, 8]. As for example, Surin et al. [8] showed a non-classical behaviour of the host molecule rotational constant as a function of the cluster size and suggested that the CO rotation is almost free in clusters with more than 5 ^{4}He atoms, exploring its possible relationship with their clustering at the end of the dopant molecule and the decoupling of the He motion from the molecular rotation.

Effective approaches to describe ground-state doped bosonic ^{4}He clusters include variational, diffusion and path-integral Monte-Carlo methods [9, 10, 11, 12, 13]. Extensions of these methods also provide excited-state properties [14, 15, 16, 17]. The most obvious difficulty in applying these techniques to fermionic clusters lies in the nodal structure of the wave-function arising from the anti-symmetry condition imposed by the Fermi-Dirac statistics. The fermionic sign problem is usually avoided by employing the the fixed-node Diffusion Monte-Carlo approximation [18, 19]. Using the released-node technique, an estimation of the bias introduced can be obtained [20]. Despite these handles to relieve the sign problem, there are only a few studies of fermionic doped He clusters using these methods [21, 22]. In addition, ground-state energies and one-particle densities of bosonic, fermionic and mixed He nanodroplets can be obtained through the orbital-free Density-Functional-Theory(DFT)-based treatment by, e.g., Barranco and collaborators [23]. Alternatively, wave-function-based electronic structure methods that consider ^{3}He atoms as "pseudo-

Proceedings of the International Conference of Computational Methods in Sciences and Engineering 2010 (ICCMSE-2010)
AIP Conf. Proc. 1642, 69-80 (2015); doi: 10.1063/1.4906632

electrons" and the dopant species as a structured "pseudo-nucleus" (i.e., replacing Coulomb interactions by He-He and He-dopant pair potentials) was first proposed and implemented for cases of 1 and 2 ^{3}He atoms by Jungwirth and Krylov [24] so that all the fermionic symmetry effects are automatically included and the know-how developed in electronic structure theory can be applied. However, there are a number of differences with the electronic structure problems that prevent the direct implementation of standard electronic structure methods, as for example, Hartree-Fock. Thus, whereas the electron-electron interaction is repulsive and the electron-nucleus one is attractive, both the He-He and the He-dopant interactions are sharply repulsive at short distances and weakly attractive at larger distances. This hard-core He-He repulsion at short distances is the origin of unphysical, non-bound, Hartree-Fock solutions, apart from the maximum spin cases in which the He atoms are already constrained to occupy different spatial one-particle states. As originally proposed in the application of the Hartree approach to quantum crystals by, *e.g.*, Bernardes and Primakoff in the Sixties [25], this problem is usually overcome by softening the hard-core He-He interaction at short distances [23, 26, 27]. Although, this truncation obviously makes these treatments parameter-dependent, it is worth recalling that Hartree and Hartree-Fock results obtained for Br_2 and ICl as dopant species were able to explain the key experimental results (i.e., the unstructured spectrum of the guest molecule for doped ^{3}He nanodroplets and the sharp profile in the ^{4}He ones) as caused by a high-energy degeneracy for the lowest solvent spin states in doped ^{3}He clusters, which is absent in the spinless ^{4}He case [26, 28, 29, 30, 31]. To take the next steps forward, it is important to assess the accuracy of approaches with a softened He-He core as well as to establish benchmarks in the development of new ones to describe excited solvent states. With this goal in mind, we developed a Full-Configuration-Interaction (FCI) implementation in which, by extension of the quantum-chemistry (QC) notation, the one-particle He states are called "nuclear orbitals" (NO). The FCI-NO treatment, as compared to other QC-like approaches, thus explicitly deals with the hard-core problem, and captures fine short-range correlation effects. An outline of the implementation, including methodological and computational aspects which have not previously published, is given in Section 2. In a series of papers [32, 33, 34, 35, 36] the FCI-NO method was applied to ^{3}He clusters containing Br_2 [32, 35] and Cl_2 [33, 34, 36], in both the ground and the excited electronic states, as the dopant species, and using semiempirical T-shaped as well as *ab initio* He-dopant with minima on both T-shaped and linear configurations [36]. They are systems in which the He-dopant interaction dominates over the He-He one, with the host molecule embedded within the ^{3}He cluster. Numerical tests were also carried out by multiplying the He-He potential in such a way that the strengths for He-molecule and He-He interactions become similar [35]. A selection of results is overviewed in Section 3.

An enhanced version of the FCI-NO code was recently developed to also deal with bosonic systems so that doped ^{4}He clusters can be handled on an equal footing. As an illustrative application, preliminary results on $(^4\text{He})_N$-$Cl_2(X)$ clusters, with $N \leq 4$, are provided in Section 4.

THEORETICAL APPROACH

Quantum-Chemistry-like Approach

Considering the particular case of a diatomic molecule, AB, in the N ^{3}He atom environment and working with satellite coordinates $(\mathbf{r}, \mathbf{R_k})$ with $\mathbf{r}$ as the vector joining the atoms of the diatomic and $\mathbf{R_k}$ as the vector from its center of mass to the different ^{3}He atoms, a body-fixed (BF) coordinate system with the Z axis parallel to the molecular axis was chosen. Keeping the diatomic bond length fixed, as in electronic structure problems, the Schrödinger equation of the N ^{3}He atoms clustering the diatomic molecule is first solved, e.g., [26];

$$\left[H^{(N)} - E^{(N)}_{\Lambda,S}(r)\right] \Phi^{(N)}_{\Lambda,S}(\{\mathbf{R}_k\}, \{\sigma_k\}; r) = 0 \tag{1}$$

where S is the total spin angular momentum of the He atoms. $H^{(N)}$, the analog to the electronic Hamiltonian can be written as:

$$H^{(N)} = \sum_{k=1}^{N} \left(K_k(\mathbf{R_k}) + V_k^{\text{AB-He}}(\mathbf{R_k}; r)\right) + \sum_{k \leq l} V_{kl}^{\text{He-He}}(|\mathbf{R}_k - \mathbf{R}_l|) - \frac{\hbar^2}{m_{AB}} \sum_{k<l} \nabla_k \cdot \nabla_l \tag{2}$$

$H^{(N)}$ thus comprises one-particle kinetic, K_k, and potential energy terms, $V_k^{\text{AB-He}}$, as well as two-particle potential, $V_{kl}^{\text{He-He}}$, and kinetic energy coupling, $\nabla_k \cdot \nabla_l$, terms. The r-dependent eigenvalues and eigenfunctions are labeled according to the projection of the total He orbital angular momenta $\mathbf{L}=\sum_N \mathbf{l}_k$ on the molecular axis Λ and S. For a total angular momentum $\mathbf{J}=\mathbf{j}+\mathbf{L}+\mathbf{S}$ ($\mathbf{j}$ being the diatomic angular momentum) with a projection onto the BF Z-axis

$\Omega = \Lambda + \Sigma$ (Σ being the projection of S on Z), omitting Coriolis couplings, the modified Hamiltonian of the dopant molecule can be written as,

$$H_N^{eff} = -\frac{\hbar^2}{2m}\frac{\partial^2}{\partial r^2} + U(r) + E_{\Lambda,S}^{(N)}(r) + \frac{\hbar^2}{2mr^2}\langle \mathbf{j}^2 \rangle. \tag{3}$$

It should be noticed that there is an additional potential energy term coming from the r-dependent total energies of the solvent states. The effect of the He environment is also reflected on the rotational molecular term $\langle \mathbf{j}^2 \rangle$. Since $\mathbf{L}$ is not a good quantum number, $\mathbf{j}^2$ is averaged over the total helium wave-function,

$$\langle \mathbf{j}^2 \rangle \approx J(J+1) + S(S+1) + \langle \Phi_{\Lambda,S}^{(N)}(\{\mathbf{R}_k\},\{\sigma_k\};r)|\mathbf{L}^2|\Phi_{\Lambda,S}^{(N)}(\{\mathbf{R}_k\},\{\sigma_k\};r)\rangle - 2(\Lambda^2 + \Sigma^2 + \Lambda\Sigma). \tag{4}$$

In turn, since the total angular momentum square is a two-particle property (i.e., the orbital angular momenta of different He atoms are coupled) a wave-function-based method is needed to obtain it, or at least, approaches capable of providing the second-order reduced density matrix. Explicitly,

$$\langle \Phi_{\Lambda,S}^{(N)}(\{\mathbf{R}_k\})|\mathbf{L}^2|\Phi_{\Lambda,S}^{(N)}(\{\mathbf{R}_k\})\rangle = \sum_{ijkl} L_{ij}L_{kl}\Gamma_{ij;kl} + \sum_{ij} L_{ij}^2\gamma_{ij} \tag{5}$$

with Γ and γ as the standard two-particle and one-particle reduced density matrices in the chosen one-particle basis set, L_{ij} and L_{ij}^2 being, respectively, the matrix representation of the total He angular momentum operator and its square on that basis. The modified Schrödinger equation $\left[H_N^{eff} - \varepsilon_{JS\Lambda\Sigma v}\right]\chi_{JS\Lambda\Sigma v}(r) = 0$ is then solved to calculate the dopant eigenvalues and rovibrational Raman spectra (see below). The ansatz for the total wave-function of the system can be therefore written as,

$$\mathscr{F}_{\Lambda S\Sigma v}^{JM(N)} = \chi_{JS\Lambda\Sigma v}(r)\Phi_{\Lambda,S}^{(N)}(\{\mathbf{R}_k\},\{\sigma_k\};r)\mathscr{D}_{M\Omega}^{J^*}(\varphi_r,\theta_r,0) \tag{6}$$

where $\mathscr{D}_{M\Omega}^{J^*}(\varphi_r,\theta_r,0)$ are Wigner rotation matrices depending on the $\mathbf{r}$ polar components in the space-fixed (SF) frame.

The main approximations involved in this QC-like model are therefore: (1) the pair-wise approach for the global potential energy surface; (2) the adiabatic approach for the diatomic stretch mode; (3) the decoupling of the diatomic rotation from the He motion. The validity of the pair-wise approach along with the adiabatic approximation has been confirmed by *ab-initio* and variational calculations on complexes with two ^{4}He atoms [37, 38, 39, 40]. The approximation of decoupling the molecular rotation has also been tested for heavy as well as light host molecules [37, 38]. In any case, it is worth stressing that the Coriolis non-adiabatic coupling terms between quantum-chemistry-like He states, induced by the molecular rotation, can be dealt with later within this approach, e.g. [41].

Full-configuration-interaction Nuclear Orbital Implementation

The hardest part of a practical calculation is obviously solving Eq. 1. As in typical electronic structure problems, one-particle basis sets comprising spherical harmonics $Y_{\ell m}(\theta,\phi)$ were adopted. Instead of the common Gaussians we employ radial functions that are obtained by numerically solving the Schrödinger equation of the He-AB triatomic at fixed angular orientations θ. Explicit integral expressions in this one-particle representation have been provided in Ref. 27. The integral evaluation program was interfaced to an efficient FCI code, which is a modified version of the DYNAMIC CI program [42]. This FCI program is based on configuration state functions (CSFs) and is optimized for a small number of fermions. Expressions for the coupling coefficients in the CSF basis can be found, e.g., in Ref. 43.
In this one-particle (CFS) representation, the generic basis wave function of N fermions is

$$\Psi = D\hat{A}\{\phi_1(\mathbf{R}_1)\phi_2(\mathbf{R}_2)\ldots\phi_N(\mathbf{R}_N)\,\Xi_{S\Sigma}^a(\sigma_1,\sigma_2,\ldots,\sigma_N)\}, \tag{7}$$

where D is the normalization factor, $\hat{A}$ is the anti-symmetrization operator with respect to the interchange of both spatial $\mathbf{R}_i$ and spin σ_i coordinates; ϕ_i are spatial-only one-particle orbitals, $\Xi_{S\Sigma}^a$ is the $a-th$ spin function (CSF) for N fermions corresponding to the total spin S and its projection Σ. In this implementation the CSFs are constructed in the same way as in the MOLPRO program package [44]: they are genealogical wave functions, ordered according to an inverse lexical order [45, 46].

The spatial one-particle functions, $\phi(R_i)$, used to construct the CSFs are linear combinations of the original "atomic" orbitals. A transformation of the integrals to these orbitals which are selected to provide better convergence of the

iterative FCI procedure, is performed before the FCI run. In practice, starting with the smallest basis set size, the initial orbitals are derived from the diagonalization of the Hamiltonian corresponding to an independent-particle approximation. Next, we used an increasing-orbital-space technique in which the FCI vectors obtained for each cluster size, spacial symmetry and spin value from the previous calculation with a smaller basis are projected on an expanded representation space. These FCI vectors are used as initial guesses in the iterative diagonalization. We found that this strategy significantly accelerates the convergence of the iterative FCI treatment.

Due to the large size of the FCI configuration space, it is only possible to use the so called "direct-CI" iterative methods, where the matrix to diagonalize is never evaluated and stored, but rather its action on a given trial vector is provided. In electronic structure calculations the Davidson method [47] is the most commonly used iterative eigensolver. Its advantage is that no additional matrix– vector operation is needed for a given iteration. The Davidson algorithm belongs to the family of the Krylov-space methods. In these approaches, the current approximation $\vec{v}$ to the eigenvector of Hamiltonian $\hat{H}$ is obtained by diagonalizing the Hamiltonian in the Krylov subspace $\{\vec{v}_1, \vec{v}_2 \ldots \vec{v}_n\}$. The current approximation to eigenvalue is given by $E = \langle \vec{v}|\hat{H}|\vec{v}\rangle$. Further, the Krylov subspace is expanded by adding vector $\hat{D}\vec{r}$ where $\vec{r}$ is a residual vector, $\vec{r} = (\hat{H} - E)\vec{v}$, and $\hat{D}$ is a pre-conditioning operator. In the standard Davidson approach $\hat{D}$ is taken in a simple diagonal form,

$$\hat{D} = \hat{Q}(\hat{H}_d - E)^{-1}\hat{Q}, \tag{8}$$

where $\hat{Q}$ is the orthogonal projector, $\hat{Q} = \hat{1} - |\vec{v}\rangle\langle\vec{v}|$, and $\hat{H}_d$ is the diagonal of Hamiltonian in the basis used to express vectors, $\hat{H}_d = diag(\hat{H})$. Note that if we would be able to solve a similar equation with full Hamiltonian instead of its diagonal, $\vec{v}_{n+1} = \left(\hat{Q}(\hat{H} - E)\hat{Q}\right)^{-1}\vec{r}$ or, equivalently

$$\hat{Q}(\hat{H} - E)\hat{Q}\vec{v}_{n+1} = \vec{r}, \tag{9}$$

this would result in a method similar to the inverse iteration method, which is known to have extremely fast convergence rate for nearly any type of matrix, and independently on the vector basis used. Unfortunately, the solution of this linear equation is as difficult as the solution of the eigenvalue problem itself. The success of the Davidson algorithm in QC problems is due to the typical strong diagonal dominance of the electronic Hamiltonian matrices, the diagonal approximation to the Hessian, $(\hat{H} - E)$, being quite good and providing good convergence properties (20 to 30 iterations). In contrast, due to the hard-core He-He interaction, very large off-diagonal Hamiltonian elements appear in our case and, as a result, it was not possible to achieve convergence through the Davidson algorithm (even after 30000 iterations) [32, 33]. Recently, we showed that the hard-core repulsion does not represent a serious problem once the Davidson algorithm is replaced by a Jacobi-Davidson modification. In the Jacobi-Davidson method, one solves the updated equation, Eq. (9), iteratively for each Davidson macro iteration. It converges quickly (350 outer Jacobi-Davidson iterations at the worst), the incorporation of the increasing-orbital-space technique providing even more rapid convergence. In the FCI program, the iterative SYMMLQ solver without any pre-conditioner was used [48]. This solver is again of Krylov type and we found that it has somewhat superior convergence in our case as compared to the MINRES [48] one.

For extremely large-scale FCI calculations it was found necessary to use a parallel implementation of the method. The reason, apart from speeding up the calculations, is that the main memory storage available for a given single CPU is not sufficient to store all the intermediate vectors and other quantities (sigma-vectors) required for the Davidson algorithm. Therefore the mixed hand-coded paradigm was adapted with both memory and work distributed over different CPUs. Both CI-vectors, sigma-vectors and two-particle integrals are distributed over CPUs on a run-time basis. Clearly, this creates noticeable overhead and requires fast inter-CPU network connection. A more efficient solution consisted in using a mainframe computer with a large amount of RAM, and employ OPENMP optimized versions of "blas" libraries. Since our Davidson algorithm is formulated in such a way that most of the work is done using blas matrix multiplication routine (DGEMM) the OPENMP blas provides quite good parallelization. This allowed the use of much larger basis sets [34]. Presently, the FCI-NO implementation allows the calculation of different one- and two-particle properties as, for example, radial and angular pair density distributions, spin densities, and magnitudes depending on the He angular momenta and its coupling with the dopant molecular rotation. Methodological details for their calculations were provided in [34].

Rovibrational Raman Spectra

In order to calculate the rovibrational Raman spectra, the same approach as in [26] was adopted. Hence, only the most relevant aspects are kept for further discussion. We assume linearly polarized incident light, propagating along the SF Y axis, and detection along the X axis. For a fixed energy of the incident photon, a Boltzmann distribution over ground as well as excited solvent states at a given temperature and an average over the initial rotational states is considered. Therefore, a line of intensity,

$$I_{fi}(T) \propto \frac{e^{-(\varepsilon_i/kT)}}{\sum_i e^{-(\varepsilon_i/kT)}} \frac{1}{2J_i+1} \sum_{M_i} |\mu_0^{f,i}|^2 \tag{10}$$

would appear at an energy $\hbar\omega_{fi} = \hbar\omega_0 - (\varepsilon_i - \varepsilon_f)$ of the scattered photon, i (f) being a collective index denoting the quantum numbers of the initial (final) state (i.e., $\{JS\Lambda\Sigma v\}$). The transition induced dipole moment $\mu_0^{f,i}$ can be expressed in terms of the spherical $\alpha_{f,i} = (\alpha_0^{f,i} + 2\alpha_1^{f,i})/3$ and the anisotropic $\beta_{f,i} = (\alpha_0^{f,i} - \alpha_1^{f,i})$ parts of the polarizability [49] as,

$$\mu_0^{f,i} \sim \alpha_{f,i} \begin{pmatrix} J_i & 0 & J_f \\ -M_i & 0 & M_i \end{pmatrix} \begin{pmatrix} J_i & 0 & J_f \\ -\Omega_i & 0 & \Omega_f \end{pmatrix} + \frac{2\beta_{f,i}}{3} \begin{pmatrix} J_i & 2 & J_f \\ -M_i & 0 & M_i \end{pmatrix} \begin{pmatrix} J_i & 2 & J_f \\ -\Omega_i & 0 & \Omega_f \end{pmatrix}. \tag{11}$$

with $\alpha_m^{f,i} = \langle \chi_i | \alpha_m | \chi_f \rangle$ and with α_m as the diatomic polarizability. In contrast to previous studies using this approach [26, 28, 31], the r-dependence of the $E_{\Lambda,S}^{(N)}$ eigenvalues in Eq. 3 was neglected. Since we focused on the vibrational excitation $v = 1 \leftarrow 0$ of the diatomic, the relevant r range being very narrow and the energy r-dependence being very weak, this is a reasonable approximation. As in previous studies [26, 28, 31, 36], a vibrational pre-dissociation mechanism (e.g., [50]) was assumed to be responsible of line broadening. First, the VP line broadening for the He-molecule triatomic is obtained using the framework of an adiabatic angular model [51]. Hereafter, the VP line broadening of a N-sized complex is assumed to be N times that of the triatomic, $\Gamma_N/2 \sim N \times \Gamma_1/2$. This assumption was further supported by the fact that quasi-linear dependences of the FCI total energies as a function of N were obtained [33, 34, 35, 36]. Finally, the stick lines are dressed with Lorentztians of the calculated widths.

^3HE_N-DIATOMIC CLUSTERS WITH T-SHAPED INTERACTION POTENTIALS: AN OVERVIEW

Recently the FCI-NO method was applied to fermionic clusters containing $Cl_2(B)$ [33, 34], $Cl_2(X)$ [36] and $Br_2(X)$ [32, 35] as the dopant species, with typical high anisotropic He-impurity interactions, the minimum being located at a T-shaped configuration and about four or five times deeper than the He-He minimum. We first studied convergence properties upon increasing the basis set size, dealing with up to ~ 400 million configurations and 400 basis functions. As a consequence of the hard-core He-He interaction at short distance and highly anisotropic He-dopant potential, spherical harmonics comprising very high angular momentum values ($\ell_{max} \geq 8$), with $m_{max} = \ell_{max}$, had to be included to get convergence. Regardless what the dopant species is, a quasi-linear dependence of the ground-state total energies with the cluster size was found as the lowest state of the triatomic would be N-times occupied. At first glance, this was surprising because we are dealing with a fermionic system in which the ^{3}He atoms are constrained to occupy excited one-particle orbitals. This will be explained later.

A Natural Orbital Analysis

The robustness of the nuclear orbital approach was also tested by calculating the natural orbitals (i.e., the eigenvectors of the first-order reduced density matrix). The iso-probability surfaces for a cluster containing 4 ^{3}He atoms can be seen in Fig. 4 of [34]. Starting with the ring-like $1\sigma_g$ orbital, the close-lying $1\pi_u$ and $1\delta_g$ excited orbitals describe quantized rotations on the ring-plane, i.e. around the molecular axis. These natural orbitals depart slightly from the independent-particle (IP) counterparts. In the IP representation, the lowest energy levels mimic rotational energy levels of a rigid rotor on the perpendicular plane to the Z axis with energies approximatively given by $B_{eff} \times \varepsilon_0 + \ell_z^2$, where B_{eff} is an effective rotational constant that is proportional to the expectation value $\langle \frac{1}{2\mu R^2} \rangle$ on the $1\sigma_g$ state, with ε_0 as its energy, and ℓ_z is the orbital angular momentum projection on the Z axis. Overall, high fractional

occupation numbers of the natural orbitals were obtained which reflected the strong He-He correlation and the high multi-configurational character of the wave-function. Despite this, three He natural orbitals were enough to describe at the very least 91% of the He population for the largest cluster size (N=4). This highlighted the adequacy of the nuclear orbital approach.

Zeroth-order Approximation to the FCI Wave-function

By using natural orbitals, it was also found that the best representation of the FCI wave-function is obtained by using cylindric coordinates and one-particle orbitals that can be written as,

$$\psi_{v_\rho v_z m}(x,y,z) = \frac{1}{\sqrt{\rho}} o_{v_\rho v_z}(\rho,z) \frac{1}{\sqrt{2\pi}} e^{im\phi} \tag{12}$$

The orbitals o are orthonormal with respect to integration $\int_0^\infty d\rho \int_{-\infty}^\infty dz\, o_{v_\rho v_z} o_{v'_\rho v'_z} = \delta_{v_\rho v_z} \delta_{v'_\rho v'_z}$, with v_ρ and v_z as the assigned quantum numbers for vibrations along ρ and z, respectively. Using (v_ρ, v_z) notation, a given orbital is symmetric with respect to inversion of z for even v_z, and anti-symmetric for odd v_z; independently on v_ρ. It was found that the wave-function part depending on ρ and z coordinates can be described by just one in-plane orbital, meaning the ring plane perpendicular to the molecular axis and passing through its mass center, and one out-of-plane orbital (hereafter referred to as the (0,0) and (0,1) orbitals, respectively). In particular, the spatial part of the wave-function for the lowest-energy states, that are symmetric with respect to Z inversion, can be simplified to the expression: $(0,0)^N \left(\sum_I w_I \left[\prod_{i=1}^N e^{-im_i^I \phi_i} \right] \right)$, where the in-plane orbital $(0,0)$ would be occupied N-times and the azimuthal part can be written as a sum of a few reference configurations expressed as simple products of complex exponentials for the azimuthal angles of each He atom (see Table III in [34]). The same holds true for the low-lying antisymmetric-in-Z states but now with a single-occupied out-of-plane orbital [i.e., $(0,0)^{N-1}(0,1)$]. Considering the particular case of two ^{3}He atoms, the zeroth-order wave-function for low-lying symmetric-in-Z states,

$$\Phi_{\Lambda S}^{(N=2)} \sim o_1(\rho_1,z_1) o_1(\rho_2,z_2) \frac{1}{\sqrt{2\pi}} e^{i\Lambda\phi_+} f_m^{P_\phi}(\phi_-) \Xi_{S\Sigma}(\sigma_1,\sigma_2), \tag{13}$$

contains an azimuthal term depending on the half sum of the azimuthal angles, ϕ_+ describing the overall rotation around the Z axis, a spin part $\Xi_{S\Sigma}$ (written in terms of configuration state functions), and a term depending on the half difference between the azimuthal angles of the two particles, ϕ_-, written as a sum of cosine $[f_m^+(\phi_-) = \cos(m\phi_-)]$ or sine-type functions $[f_m^-(\phi_-) = \sin(m\phi_-)]$ depending on the symmetry with respect to ϕ_- inversion, $P_\phi = \pm$.

Similarly to previous studies by Villarreal et al. [52] and Hernández et al. [53] for the ^{4}He isotope, the wave-function structure in Eq. 13 can be understood by resorting to a reduced dimensional model for the half-sum and half-difference of the azimuthal angles (i.e., averaging the Hamiltonian over the doubled occupied $(0,0)^2$ orbital),

$$\langle H^{N=2} \rangle_{(0,0)} = \langle \frac{-\hbar^2}{4\mu R^2} \rangle_{(0,0)} \left[\frac{\partial^2}{\partial^2 \phi_+} + \frac{\partial^2}{\partial^2 \phi_-} \right] + \langle V^{\mathrm{He-He}}(2\phi_-) \rangle_{(0,0)} \tag{14}$$

where μ is the reduced ^{3}He-diatomic mass. In this way, the reduced Hamiltonian term depending on ϕ_+ would be correlated to quantized overall rotations around the Z-axis with a frequency $\sim B_{\mathrm{eff}}/2$. On the other hand, the eigenvectors of the Hamiltonian term depending on ϕ_-, owing to the hard-core He-He interaction, mimic particle-in-a-box states. This can be generalized to the larger cluster sizes considered: the azimuthal part of the wave-function describes particle-in-a-box-like states along with overall quantized rotation around the Z axis.

A Pair Density Distribution Analysis: Short-range Correlation Effects

A pair density distribution analysis can reveal additional fine correlation effects and further clarify the wave-function structure. By comparing, for example, Fig. 5 of [53] and the upper panel in Fig. 5 of [36], it can be seen how the angular pair density distributions of the low-lying symmetric-in-Z states resemble the lowest- and the first-excited particle-in-a-box-like state. However, the distributions have also a shoulder at a close angle ($\gamma_{12} \sim 70°$). This correlates with a feature in the radial pair density distribution that enters a little bit on the attractive region of the He-He potential (see,

e.g., Fig. 7 of [34]). As a consequence, the average He-He interaction is negative (see Fig. 1 (b) in [34]). As the cluster size increases the shoulder becomes more pronounced, and a true local maximum for four ^{3}He atoms (see Fig. 7 of [34]). It was also found that the most probable structure is not the classical one of N ^{3}He atoms equally spaced on the ring plane, but there is some sort of structural "pairing" of the ^{3}He atoms on a plane containing the molecular axis and the perpendicular plane to that axis, as well. The average He-He attractive energy scales as a power of 3 with a number of ^{3}He atoms. Very similar rates were found for $Br_2(X)$ and $Cl_2(X,B)$ host molecules. These results are interesting if taking into account that the He-He potential does not support bound states in the fermionic case. In short: the impurity is not only able of holding together the otherwise unbound ^{3}He atoms but also of inducing their structural pairing to benefit from the weak minimum of the He-He potential. The origin of the shoulder was further clarified by carrying out a numerical test by multiplying the He-He interaction in such a way that the strengths for He-molecule and He-He interactions become similar [35]: the peak of the pair density distributions shifted to the position of the shoulder, highlighting the fact that its origin is at the minimum of the He-He potential (inset in Fig. 2 of [35]).

Global Analysis

Overall, the quasi-linear behaviour of the binding-energies as a function of the cluster size can be rationalized as a balance between the progressively less attractive one-particle part, due to the filling of excited one-particle orbitals that raises the global kinetic energy but keep the He-dopant interaction as N times the one for a single particle, and the increasingly more attractive He-He part coming from long wave-function tails that penetrate into the minimum region of the He-He potential. In all fermionic cases analysed, the ground states were found for Σ-type states. A high degree of degeneracy was also found for the lowest spin states and that the larger the cluster size, the smaller the promotion energies to the low-lying excited states. These lowest spin states share nearly identical one- and two particle distributions. In fact, a further analysis shows that the excitation mode is mainly on the overall quantizied rotation around the Z axis. As can be deduced by generalizing Eq. 14 to larger cluster sizes, the frequency for this motion would be $\sim B_{eff}/N$, which obviously decreases as the cluster size increases. Conversely, the hard-core of the effective He-He interaction is intensified when augmenting the number of ^{3}He atoms in such a way that the excited particle-in-a-box-like levels become higher in energy. It is also worth mentioned that, as can be noticed from Eq. 14, the spin term in the antisymmetric ^{3}He wave-function provides a less stringent constraint for the allowed global rotational levels around the Z axis $e^{i\Lambda\varphi_+}$ than in the spin-less ^{4}He case. In order to analyze how these global results are reflected on the rovibrational Raman spectra, a Cl_2 molecule in the ground electronic state was considered, by using first a T-shaped model He-molecule potential function [36]. By comparing the spectra for different cluster sizes (see Fig. 7 of [36]), it can be noticed that the profile is increasingly more congested as the cluster grows in size because additional contributing lines appear, mainly coming from near degenerated spin multiplets, which gives rise to peaks of comparable intensities. Actually, not only the lowest spin states contribute to the spectrum but also other low-lying states describing quantized overall rotation around the Z axis. In any case, a decongested spectrum is recovered when the temperature is lowered to 0.1 K and only the ground $^1\Sigma_g^+$ state contributes.

It is worth stressing that the main conclusion obtained by using a Hartree-Fock model with a softened He-He core is corroborated by our FCI calculations. Thus, Hartree-Fock results predicted a high-degree of degeneracy for the lowest-spin states [26, 30] and, then, qualitatively explain one of the crucial experimental findings at temperatures in which doped ^{4}He nanodroplets are superfluid (i.e., a congested spectrum in doped ^{3}He clusters [54]). The qualitative agreement is attributed to the fact that short-range correlation effects are very similar within the lowest-energy manifold of states which, as a matter of fact, share almost identical pair densities. Quantitatively, Hartree-Fock energies were found to be moderately underestimated, with the relative errors oscillating between 2 and 12% [35].

BOSONIC ^4HE_N-$CL_2(X)$ CLUSTERS: PRELIMINARY RESULTS

Very recently, a FCI-NO implementation that also deal with bosonic systems was worked out [55]. The extension is applied here to ^{4}He clusters containing $Cl_2(X)$ as the dopant species. The analytical form of the PES was obtained from the CCSD(T) data reported by Cybulski and Holt [56] by using a Legendre polynomial expansion in θ and a fitting to Morse-var der Waals functions in R [57]. This PES comprises two minima (see inset panel of Fig. 1): a global minimum of ~ -45.8 cm^{-1} at a linear configuration (R_e=4.16 Å) and a secondary minimum at a T-shaped configuration of ~ -44.2 cm^{-1} (R_e=3.39 Å). For comparison purposes, calculations for the ^{3}He case were also carried out.

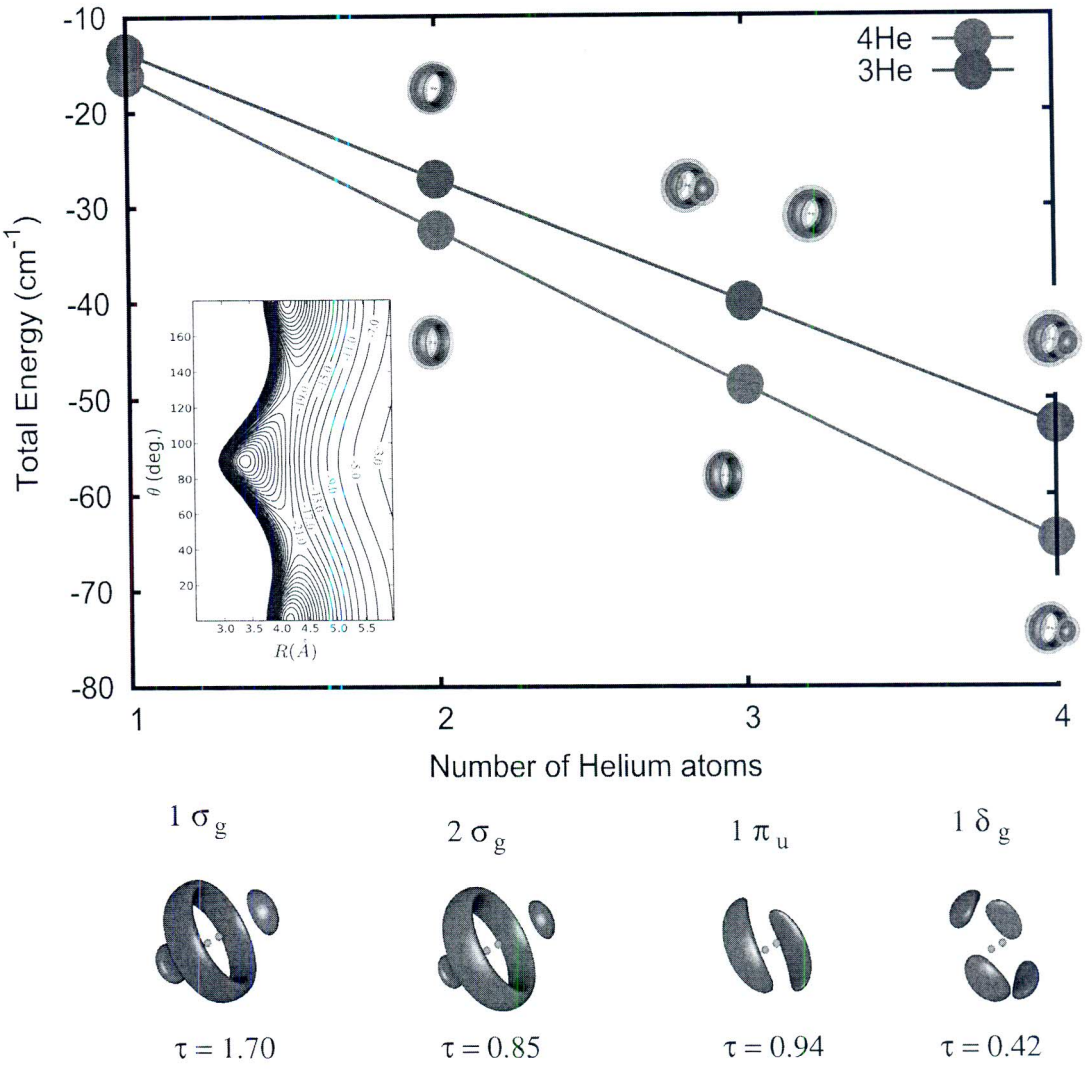

FIGURE 1. FCI energies (in cm^{-1}) of the ground ^{3}He and ^{4}He states in He-$Cl_2(X)$ clusters. Equiprobabilities density surfaces between $0.01 \times max\{|\rho^{gs}|^2\}$ and $0.5 \times max\{|\rho^{gs}|^2\}$ are also depicted. Inset: Contour plots of the He-$Cl_2(X)$ PES as a function of the distance of the He atom from the Cl_2 center of mass (R) and θ, the angle that **R** forms with the bond direction. Bottom panel: Equiprobability density surfaces and occupation numbers of the relevant natural orbitals for N=4 and the ^{4}He isotope. Red and blue colors indicate positive and negative lobes of the orbitals, respectively. The probability values have been selected to be the half the maximum value attained at each natural orbital.

As can be seen in Fig. 1, the apparent global energetic aspects of the ground ^{4}He states do not differ too much when compared to the fermionic case. Thus, ground-state energies behave quasi-linearly with the number of ^{4}He atoms and, as expected due to the heavier mass of the ^{4}He isotope, are lower. The lowest-energy states are also of Σ symmetry and the average pair He-He energies are negative but scale with a larger constant rate for ^{4}He atoms. Actually, the energies are a bit lower than N ground-state tri-atomics, in contrast with the fermionic case. This seems natural if considering that pure ^{4}He clusters are bound, independently of the number of He atoms. Our results are in line with the previous study carried out by Bačić et al.[58] on $(^4He)_N$-$Cl_2(B)$ clusters ($N \leq 3$), using the Green's function Monte-Carlo method, in which a simple additive model for the total energies, as a sum of independent N ^{4}He-Cl_2 and $N(N-1)/2$ $^4He_2$ oscillators, was proposed. The quasi-linear behaviour of ground-state energies was also found on $(^4He)_N$-$Br_2(X)$

clusters ($N \leq 5$) through a configuration-interaction treatment for $J = 0$ by Felker [59].

Let us now see how the impurity is solvated by the He atoms. Although the linear minimum of the He-dopant PES is deeper, zero point energies reverse the order of stabilities in such a way that a belt around the molecular axis is filled first (see Fig. 1). However for four He atoms and both isotopes, the ground-state density flows towards the chlorine ends, in such a way that the dopant becomes fully coated. The transition to the full-coated regime is also apparent when analysing the average He-He energy which no longer scales as a power of three with the number of He atoms but quasi-linearly. In fact, it occurs when the increased average kinetic energy for ring-like states is not counterbalanced by the higher He-He attractive interaction within the ring plane. Due to the lighter mass of the ^{3}He isotope, the densities are more delocalized and the clustering of the ^{3}He atoms at the Cl_2 ends is already apparent in excited solvent states that are almost degenerated with the ground-state for N=3, as the one whose density is represented in Fig. 1 along with the ring-shaped density corresponding to the lowest-energy state.

The FCI wave-function make-up of bosonic clusters was also analyzed, after rotating it to the basis of natural orbitals. Independently of the cluster size, the main contribution comes from the permanent (i.e., a symmetrized Hartree product of one-particle orbitals) where all the bosons reside in the first natural orbital (i.e., the $1\sigma_g$ orbital). The absolute values of the associated coefficients, however, decrease rapidly from ~ 0.9 for N=2 to ~ 0.5 for N=4. In fact, for N=4, the contribution from the $(1\sigma_g)^2(2\sigma_g)^2$ and $(1\sigma_g)^3(2\sigma_g)^1$ permanents becomes already significant (~ 0.3 and 0.2, respectively). The fragmentation of the condensed solution, with all the ^{4}He occupying the same orbital, reflects, on the one hand, the transition to the full-coated regime, which is also apparent from the mixing of the independent-particle ($1\sigma_g$) and ($2\sigma_g$) orbitals (see Fig. 1). The depletion of the $1\sigma_g$ orbital also takes places through the promotion to the $1\pi_u$ orbital (see Fig. 1), with an occupation number that increases from 0.24 for N=2 to 0.92 and 0.94 for N=3 and 4, respectively. In an effective one-particle picture this could be explained by taking into account that the on-site interaction on the ring-like $1\sigma_g$ orbital is increasingly more repulsive as the ring becomes more crowded.

Rovibrational $Cl_2(X)$ Raman Spectra in ^{4}He Clusters

In order to perform the spectra simulations, temperatures of 2 and 0.37 K were considered, including values for the total angular momentum $J \leq 10$ to achieve convergence. Accurate $Cl_2(X)$ polarizabilities, assumed to be unchanged by the presence of He atoms, were taken from the work carried out by Maroulis [60]. The more intense Q ($\Delta J = 0$) branches are shown in Fig. 2, which displays continuum profiles of the scattered photon intensity as a function of the energy loss between the incident and the exiting photons, $\hbar w_0$ - $\hbar w_{fi}$, measured with respect to the bare dopant forbidden transition (J,v)=(0,1) $\leftarrow$ (0,0), 554.37 cm^{-1}. The main lines contributing to the different profiles are specified as (J,Ω) where J=J_i. Note that Ω=Λ for ^{4}He zero-spin atoms. Focussing on the spectra at T=2 K, it can be observed that although the most intense lines are associated to the lowest Σ states [e.g., the one with (J,Ω)=(0,0)], the intensities of the lines coming from $\Omega > 0$ states are clearly significant and, therefore, the spectra appear rather congested. This seems to be in contrast with previous results by using the Hartree method [26, 28, 31], where a decongested spectrum was obtained for that temperature in (^{4}He)$_N$-$Br_2(X)$ clusters. From our viewpoint, this apparent discrepancy is due to the fact that excited He states with $\Omega > 0$ were not included in the simulations with the Hartree method. In fact, as can be seen in Fig. 2, if the temperature is lowered to 0.37 K (the temperature at which microscopic superfluidity was probed in ^{4}He nanodroplets [1]) and for $N > 2$, only the lowest Σ states with Ω=0 contribute to the spectra (i.e., the $\Omega \neq 0$ states are not populated) and pure Lorentzian profiles are obtained. Moreover, as was found in [26, 28] and can be deduced from Eq. 11, when $\Omega_i = \Omega_f = 0$, branches with $\Lambda J = \pm 1$ (P and R branches) become forbidden and diatomic-like selection rules, $\Lambda J = 0, \pm 2$, are recovered, quite in line with both experimental finding and Hartree-based calculations [1, 26].

Before closing this section, the reliability of the approach of omitting the Coriolis couplings will be addressed, which arise from the $J^+L^- + J^-L^+$ term of $\mathbf{j}^2$ in the bosonic case (i.e., inducing a mixing between Ω and $\Omega \pm 1$ solvent states). For example, let us consider the coupling between the lowest Σ_g and Π_g states (i.e., the $\langle \Sigma_g | L^- | \Pi_g \rangle$ term). Absolute values of 0.021, 0.032 and 0.00084 a.u. were obtained. for N=2, 3 and 4, respectively. Interestingly, these values decrease very significantly when the transition to the full-coated regime takes place. The same holds true for the remaining calculated Coriolis couplings: they are reduced to as little as a factor of five. This is in line with experimental studies [8] and path-integral Monte Carlo simulations [6, 61, 62], showing an interplay between the appearance of He density at the ends of a dopant molecule and the decoupling of the He angular momentum from the molecular motion. When considering the heavier Cl_2 dopant species, however, the decoupling is apparent before the the transition to the full-coated regime since the magnitude of the Coriolis couplings are very small anyway. For any

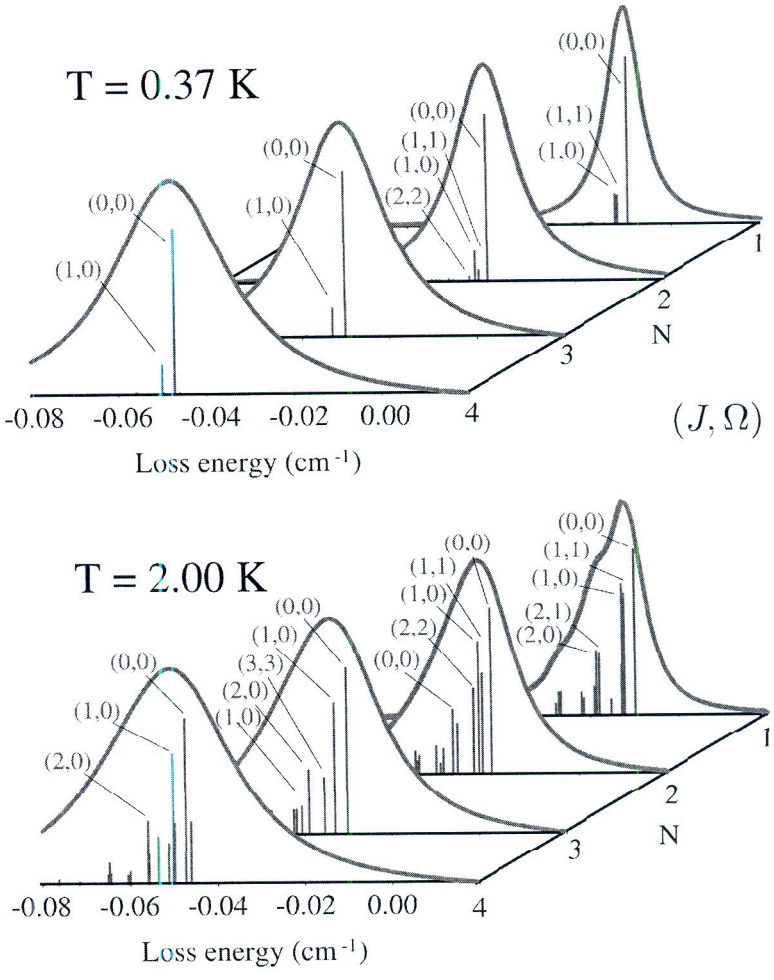

FIGURE 2. (color online) Main Q branch of the (v=1 ← 0) rovibrational Raman spectra of (^{4}He)$_N$-$Cl_2(X)$ clusters at T=2 and 0.37 K.

size, with $J \leq 10$, the mixing percentage between He states is smaller than 7%, stressing the validity of the approach of decoupling the He motion from the molecular rotation.

SUMMARY AND OUTLOOK

Methodological and computational aspects of a FCI-NO implementation to calculate ground and excited-state wave-functions of fermionic solvent species in weakly bound doped clusters has been briefly described and its application to a microscopic description of small doped ^{3}He clusters has been overviewed in this paper. Preliminary results for doped ^{4}He clusters by applying a FCI-NO implementation which deals with bosonic systems have also been presented. The global analysis of the results reveal that classical quantum chemical wave-function-based treatments to study the electronic structure of molecular systems can be properly adapted for a microscopic description of small He clusters and stress the powerful one-particle picture of these strongly correlated many-body systems. Work is in progress to make the FCI-NO treatment more efficient by implementing an optimized one-particle basis set (i.e., by using two-dimensional (ρ,z) functions and standard complex exponentials $e^{-im\phi}$) to anisotropic He-dopant potentials. The extension to mixed fermionic/bosonic systems and the work on less time-consuming but still precise methods as the multi-reference CI is also underway. The other candidates among the efficient and accurate quantum-chemistry

methods are obviously those based on coupled-cluster (CC) theory [63], provided the standard Hartree/Hartree-Fock solution is replaced by a stable zeroth-order wave function (i.e., tailored to the hard-core He-He interaction problem). Very recently, methods based on CC theory have been implemented to calculate anharmonic vibrational states [64, 65].

As a future prospect, the development of embedding schemes that have been proposed, for example, in the framework of electronic structure problems [66] to link less computationally expensive methods such as DFT to the FCI-NO treatment is considered (i.e., to allow the description of nanodroplets). The adaptation of the FCI-NO method to treat molecular or atomic species embedded in another quantum clusters is also an objective for future work. In particular, one interesting issue would be to perform a FCI wave-function analysis of ground and excited *para*-hydrogen (pH_2) states (i.e., considering pH_2 molecules as spin-less bosons) of molecule-$(pH_2)_N$ clusters inside He droplets, in connection with the recent evidences of microscopic superfluidity for certain cluster sizes [67, 68].

ACKNOWLEDGMENTS

We would like to thank M. Barranco, F. A. Gianturco, J. Jellinek, M. I. Hernández, J. Navarro, A. Hernando, N. Halberstadt, J. A. Beswick and D. López-Durán for very interesting discussions and useful suggestions. This work has been partially supported by CSIC-CM, MICINN-CSIC, and CICYT (Spain) under projects CCG08-CSIC/ESP-3680, 2007501004, and FIS2007-62006. The calculations presented here were performed at CESGA (the SuperComputer Center of Galicia), and the IFF Computer Center (CTI,CSIC).

REFERENCES

1. S. Grebenev, J. P. Toennies, and A. F. Vilesov, *Science* **279**, 2083 (1998).
2. S. Grebenev, M. Hartmann, M. Havenith, B. Sartakov, J. P. Toennies, and A. F. Vilesov, *J. Chem. Phys.* **112**, 4485 (2000).
3. J. Tang, Y. Xu, A. R. W. McKellar, and W. Jäger, *Science* **297**, 2030 (2002).
4. J. Tang, A. R. W. McKellar, F. Mezzacapo, and S. Moroni, *Phys. Rev. Lett.* **92**, 145503 (2004).
5. A. R. W. McKellar, Y. Xu, and W. Jäger, *Phys. Rev. Lett.* **97**, 18401 (2006).
6. Y. Xu, N. Blinov, W. Jäger, and P. N. Roy, *J. Chem. Phys.* **124**, 081101 (2006).
7. A. R. W. McKellar, *J. Chem. Phys.* **128**, 044308 (2008).
8. L. A. Surin, A. V. Potapov, B. S. Dumesh, S. Schlemmer, Y. Xu, P. L. Raston, and W. Jäger, *Phys. Rev. Lett.* **101**, 233401 (2008).
9. F. Paesani, A. Viel, F. A. Gianturco, and K. B. Whaley, *Phys. Rev. Lett.* **90**, 073401 (2003).
10. S. Moroni, N. Blinov, and P. N. Roy, *J. Chem. Phys.* **121**, 3577 (2004).
11. H. Li, N. Blinov, P.-N. Roy, and R. L. Roy, *J. Chem. Phys.* **130**, 144305 (2009).
12. S. Miura, *Phys. Rev. B* **126**, 114308 (2007).
13. C. Di Paola, F. A. Gianturco, D. López-Durán, M. P. de Lara-Castells, G. Delgado-Barrio, P. Villarreal, and J. Jellinek, *ChemPhysChem* **6**, 1348 (2005).
14. Z. Li, L. Wang, H. Ran, D. Xie, N. Blinov, P. N. Roy, and H. Guo, *J. Chem. Phys.* **128**, 22513 (2008).
15. S. Baroni and S. Moroni, in *Quantum Monte Carlo Methods in Physics and Chemistry*, edited by P. Nightingale, and C. J. Umrigar, NATO Series, Mathematical and Physical Sciences, Kluwer Academic, Boston, 1999, vol. 525.
16. P. Cazzatto, S. Paolini, S. Moroni, and S. Baroni, *J. Chem. Phys.* **120**, 9071 (2004).
17. K. Kwon, F. Paesani, and K. B. Whaley, *Phys. Rev. B* **74**, 174522 (2006).
18. J. D. Anderson, *J. Chem. Phys.* **63**, 1499 (1975).
19. A. B. McCoy, *Int. Rev. Phys. Chem.* **25**, 77 (2006).
20. E. Sola, J. Casulleras, and J. Boronat, *Phys. Rev. B* **73**, 092515 (2006).
21. P. Barletta, A. Fabrocini, A. Kievsky, J. Navarro, and A. Polls, *Phys. Rev. A* **68**, 053205 (2003).
22. R. Guardola, J. Navarro, D. Mateo, and M. Barranco, *J. Chem. Phys.* **131**, 174110 (2009).
23. M. Barranco, R. Guardiola, S. Hernández, R. Mayol, J. Navarro, and M. Pí, *J. Low Temp. Phys.* **142**, 1 (2006).
24. P. Jungwirth, and A. I. Krylov, *J. Chem. Phys.* **115**, 10214 (2001).
25. N. Bernardes, and H. Primakoff, *Phys. Rev.* **119**, 968 (1960).
26. D. López-Durán, M. P. de Lara-Castells, G. Delgado-Barrio, P. Villarreal, C. Di Paola, F. A. Gianturco, and J. Jellinek, *Phys. Rev. Lett.* **93**, 053401 (2004).
27. M. P. de Lara-Castells, D. López-Durán, G. Delgado-Barrio, P. Villarreal, C. Di Paola, F. A. Gianturco, and J. Jellinek, *Phys. Rev. A* **71**, 033203 (2005).
28. D. López-Durán, M. P. de Lara-Castells, G. Delgado-Barrio, P. Villarreal, C. Di Paola, F. A. Gianturco, and J. Jellinek, *J. Chem. Phys.* **121**, 2975 (2004).
29. M. P. de Lara-Castells, R. Prosmiti, D. López-Durán, G. Delgado-Barrio, P. Villarreal, C. Di Paola, F. A. Gianturco, and J. Jellinek, *Phys. Rev. A* **74**, 053201 (2006).
30. P. Villarreal, M. P. de Lara-Castells, R. Prosmiti, G. Delgado-Barrio, C. Di Paola, F. A. Gianturco, and J. Jellinek, *Phys. Scr.* **76**, C96 (2007).

31. M. P. de Lara-Castells, R. Prosmiti, D. López-Durán, G. Delgado-Barrio, P. Villarreal, F. A. Gianturco, and J. Jellinek, *Int. J. Quantum Chem.* **107**, 2902 (2007).
32. M. P. de Lara-Castells, G. Delgado-Barrio, P. Villarreal, and A. O. Mitrushchenkov, *J. Chem. Phys.* **125**, 221101 (2006).
33. M. P. de Lara-Castells, A. O. Mitrushchenkov, G. Delgado-Barrio, and P. Villarreal, *Few-Body Syst.* **45**, 233 (2009).
34. M. P. de Lara-Castells, G. Delgado-Barrio, P. Villarreal, and A. O. Mitrushchenkov, *J. Chem. Phys.* **131**, 194110 (2009).
35. M. P. de Lara-Castells, G. Delgado-Barrio, P. Villarreal, and A. O. Mitrushchenkov, *Int. J. Quantum Chem.* (2010), microscopic description of small doped ^{3}He clusters through the Full-Configuration-Interaction Nuclear Orbital approach: the $(^3\mathrm{He})_N$-$\mathrm{Br}_2(X)$ case revisited, in press, doi: 10.1002/qua.22627.
36. M. P. de Lara-Castells, N. F. Aguirre, G. Delgado-Barrio, P. Villarreal, and A. O. Mitrushchenkov, *J. Chem. Phys.* **132**, 194313 (2010).
37. O. Roncero, R. Pérez-Tudela, M. P. de Lara-Castells, R. Prosmiti, G. Delgado-Barrio, and P. Villarreal, *Int. J. Quantum Chem.* **107**, 2756 (2007).
38. O. Roncero, M. P. de Lara-Castells, G. Delgado-Barrio, P. Villarreal, T. Stoecklin, A. Voronin, and J. C. Rayez, *J. Chem. Phys.* **128**, 164313 (2008).
39. A. Valdés, R. Prosmiti, P. Villarreal, and G. Delgado-Barrio, *J. Chem. Phys.* **125**, 014313 (2006).
40. X. Wang, T. Carrington, Jr., and A. McKellar, *J. Phys. Chem. A* **113**, 13331 (2009).
41. M. P. de Lara-Castells, A. Mitrushenkov, P. Palmieri, F. L. Quére, C. Leonard, and P. Rosmus, *Mol. Phys.* **98**, 1713–1727 (2000).
42. A. O. Mitrushenkov, *Chem. Phys. Lett.* **217**, 559 (1994).
43. S. Rettrup, *Chem. Phys. Lett.* **47**, 59 (1977).
44. Molpro, version 2009.1, a package of ab initio programs designed by H.-J. Werner, P. J. Knowles, R. Lindh *et al.*, see http://www.molpro.net.
45. H. J. Werner, and P. J. Knowles, *J. Chem. Phys.* **89**, 5803 (1988).
46. P. J. Knowles, and H. J. Werner, *Chem. Phys. Lett.* **145**, 514 (1988).
47. E. R. Davidson, *J. Comput. Phys.* **17**, 87 (1975).
48. R. Barrett, M. Berry, T. Chan, J. Demmel, J. Donato, J. Dongarra, V. Eijkhout, R. Pozo, C. Romine, and H. A. Van der Vorst, *Templates for the solution of linear systems: building blocks for iterative methods*, SIAM, Philadelphia (USA), 1994.
49. E. B. Wilson, Jr., J. C. Decius, and P. C. Cross, *Molecular Vibrations: The Theory of Infrared and Raman Vibrational Spectra*, McGraw-Hill Book Company, Inc. (Reprinted by Dover Publications in 1980), New York, 1955.
50. M. P. de Lara, P. Villarreal, G. Delgado-Barrio, S. Miret-Artés, E. Buonomo, and F. A. Gianturco, *Chem. Phys. Lett.* **242**, 336 (1995).
51. J. A. Beswick, and G. Delgado-Barrio, *J. Chem. Phys.* **73**, 3653 (1980).
52. P. Villarreal, O. Roncero, and G. Delgado-Barrio, *J. Chem. Phys.* **101**, 2217 (1994).
53. M. I. Hernández, N. Halberstadt, W. D. Sands, and K. C. Janda, *J. Chem. Phys.* **113**, 7252 (2000).
54. J. P. Toennies, and A. F. Vilesov, *Angew. Chem., Int. Ed.* **43**, 2622 (2004).
55. M. P. de Lara-Castells, and A. O. Mitrushchenkov, Bosonic doped ^{4}He clusters through the Full-Configuration-Interaction Nuclear Orbital approach: a quantum-chemical perspective, unpublished.
56. S. M. Cybulski, and J. S. Holt, *J. Chem. Phys.* **110**, 7745 (1999).
57. A. Valdés, R. Prosmiti, P. Villarreal, G. Delgado-Barrio, and H.-J. Werner, *J. Chem. Phys.* **126**, 204301 (2007).
58. Z. Bačić, M. Kennedy-Mandziuk, J. M. Moskowitz, and K. E. Schmidt, *J. Chem. Phys.* **97**, 6472 (1992).
59. P. M. Felker, *J. Chem. Phys.* **125**, 184313 (2006).
60. G. Maroulis, *Mol. Phys.* **77**, 1085 (1992).
61. F. Paesani, K. Kwon, and K. B. Whaley, *Phys. Rev. Lett.* **94**, 15401 (2005).
62. S. Moroni, A. Sarsa, S. Fantoni, K. E. Schmidt, and S. Baroni, *Phys. Rev. Lett.* **90**, 143401 (2003).
63. J. Čížek, and J. Paldus, *Int. J. Quantum Chem.* **5**, 359 (1971).
64. O. Christiansen, *J. Chem. Phys.* **120**, 2149 (2004).
65. S. Banik, S. Pal, and M. D. Prasad, *J. Chem. Phys.* **129**, 134111 (2008).
66. T. Wesolowski, and A. Washell, *J. Phys. Chem.* **97**, 8050 (1993).
67. S. Grebenev, B. G. Sartakov, J. P. Toennies, and A. F. Vilesov, *J. Chem. Phys.* **132**, 064501 (2010).
68. H. Li, R. J. Le Roy, and A. R. W. McKellar, *Phys. Rev. Lett.* **105**, 133401 (2010).